Article

Current Biology

A WOX/Auxin Biosynthesis Module Controls Growth to Shape Leaf Form

Graphical Abstract

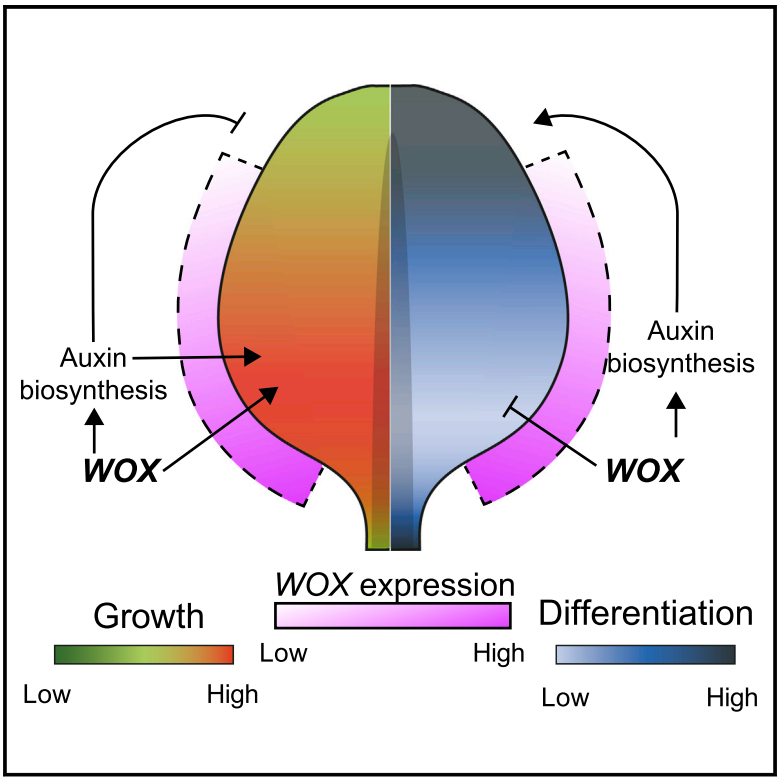

Authors

Zhongjuan Zhang, Adam Runions, Remco A. Mentink, ..., Xiangchao Gan, Karin Ljung, Miltos Tsiantis

Correspondence

tsiantis@mpipz.mpg.de

In Brief

Zhang et al. discover that a genetic module comprising WOX homeobox proteins and the hormone auxin shapes *Arabidopsis* leaf form. They find that WOXes promote auxin biosynthetic gene expression. By using time-lapse imaging, they also show that this module generates a proximodistal gradient of growth that helps leaves grow laterally.

Highlights

- *WOX1*, *3*, and *5* are required redundantly for lateral leaf growth and auxin biosynthesis
- *YUC1* expression can partially bypass the requirement for *WOX* genes in leaf growth
- Time-lapse imaging allows quantitation of *WOX* effects on leaf growth
- *WOX*es shape a growth gradient that underlies the *A. thaliana* ellipsoid leaf shape

Zhang et al., 2020, Current Biology *30*, 4857–4868
December 21, 2020
https://doi.org/10.1016/j.cub.2020.09.037

CellPress

Current Biology

CellPress
OPEN ACCESS

Article

A WOX/Auxin Biosynthesis Module Controls Growth to Shape Leaf Form

Zhongjuan Zhang,[1,4] Adam Runions,[1,5] Remco A. Mentink,[1,6] Daniel Kierzkowski,[1,7] Michal Karady,[2,3] Babak Hashemi,[1] Peter Huijser,[1] Sören Strauss,[1] Xiangchao Gan,[1] Karin Ljung,[2] and Miltos Tsiantis[1,8,*]

[1]Department of Comparative Development and Genetics, Max Planck Institute for Plant Breeding Research, Carl-von-Linné-Weg 10, 50829 Cologne, Germany

[2]Umeå Plant Science Centre, Department of Forest Genetics and Plant Physiology, Swedish University of Agricultural Sciences, 90183 Umea, Sweden

[3]Laboratory of Growth Regulators, Institute of Experimental Botany of the Czech Academy of Sciences and Faculty of Science of Palacký University, Šlechtitelů 27, 78371 Olomouc, Czech Republic

[4]Present address: Laboratory of Biochemistry, Wageningen University & Research, Stippeneng 4, 6708 Wageningen, the Netherlands

[5]Present address: Department of Computer Science, University of Calgary, 602 ICT Building, 2500 University Drive NW, Calgary, AB T2N1N4, Canada

[6]Present address: Bejo Zaden B.V., Trambaan 2A, 1749 Warmenhuizen, the Netherlands

[7]Present address: Plant Biology Research Institute, Department of Biological Sciences, University of Montreal, Montreal, QC H1X 2B2, Canada

[8]Lead Contact

*Correspondence: tsiantis@mpipz.mpg.de

https://doi.org/10.1016/j.cub.2020.09.037

SUMMARY

A key challenge in biology is to understand how the regional control of cell growth gives rise to final organ forms. Plant leaves must coordinate growth along both the proximodistal and mediolateral axes to produce their final shape. However, the cell-level mechanisms controlling this coordination remain largely unclear. Here, we show that, in *A. thaliana*, *WOX5*, one of the *WUSCHEL-RELATED HOMEOBOX* (*WOX*) family of homeobox genes, acts redundantly with *WOX1* and *WOX3* (*PRESSED FLOWER* [*PRS*]) to control leaf shape. Through genetics and hormone measurements, we find that these WOXs act in part through the regional control of *YUCCA* (*YUC*) auxin biosynthetic gene expression along the leaf margin. The requirement for WOX-mediated *YUC* expression in patterning of leaf shape cannot be bypassed by the epidermal expression of *YUC*, indicating that the precise domain of auxin biosynthesis is important for leaf form. Using time-lapse growth analysis, we demonstrate that WOX-mediated auxin biosynthesis organizes a proximodistal growth gradient that promotes lateral growth and consequently the characteristic ellipsoid *A. thaliana* leaf shape. We also provide evidence that WOX proteins shape the proximodistal gradient of differentiation by inhibiting differentiation proximally in the leaf blade and promoting it distally. This regulation allows sustained growth of the blade and enables a leaf to attain its final form. In conclusion, we show that the WOX/auxin regulatory module shapes leaf form by coordinating growth along the proximodistal and mediolateral leaf axes.

INTRODUCTION

How gene activity translates into distinct organ morphologies in complex eukaryotes remains poorly understood [1, 2]. Resolving this problem requires us to characterize the genetic modules that control different aspects of form and to understand how they influence the amount, direction, and duration of growth to shape final organ geometry [3]. Plant leaves are an attractive system in which to address these questions as they grow from almost indistinguishable leaf buds into shapes that vary tremendously among species. Leaves of eudicot plants typically emerge as peg-like protrusions from the pluripotent shoot apical meristem (SAM). Leaves can be simple with undivided margins, or complex with protrusions of different size and geometry. Yet even in simple leaf species, regulated growth along the proximodistal (PD) and mediolateral (ML) axes results in a variety of shapes, such as elliptical in the model plant *A. thaliana*, lanceolate in willow, cordate in poplar, and linear in rosemary (Figure 1A). Recent work has uncovered broad principles as to how divergent leaf shapes emerge [1, 3–6]. However, there remain substantial gaps in our understanding of how genetically regulated growth produces key elements of leaf shape. For example, it remains unclear how regional differences in growth patterns emerge and contribute to the overall shape of the leaf blade, even for the simple ellipsoid form of *A. thaliana* leaves. Theoretical models derived from time-lapse imaging indicate that a basally emanating morphogen may shape *A. thaliana* leaf form, by influencing the amount and direction of cellular growth. However, it is unclear what specific genetic modules contribute to the gradient of lateral blade growth hypothesized in such models [3, 7].

In *Arabidopsis*, members of the *WUSCHEL-RELATED HOMEOBOX* (*WOX*) gene family, *WOX1* and *PRESSED FLOWER*

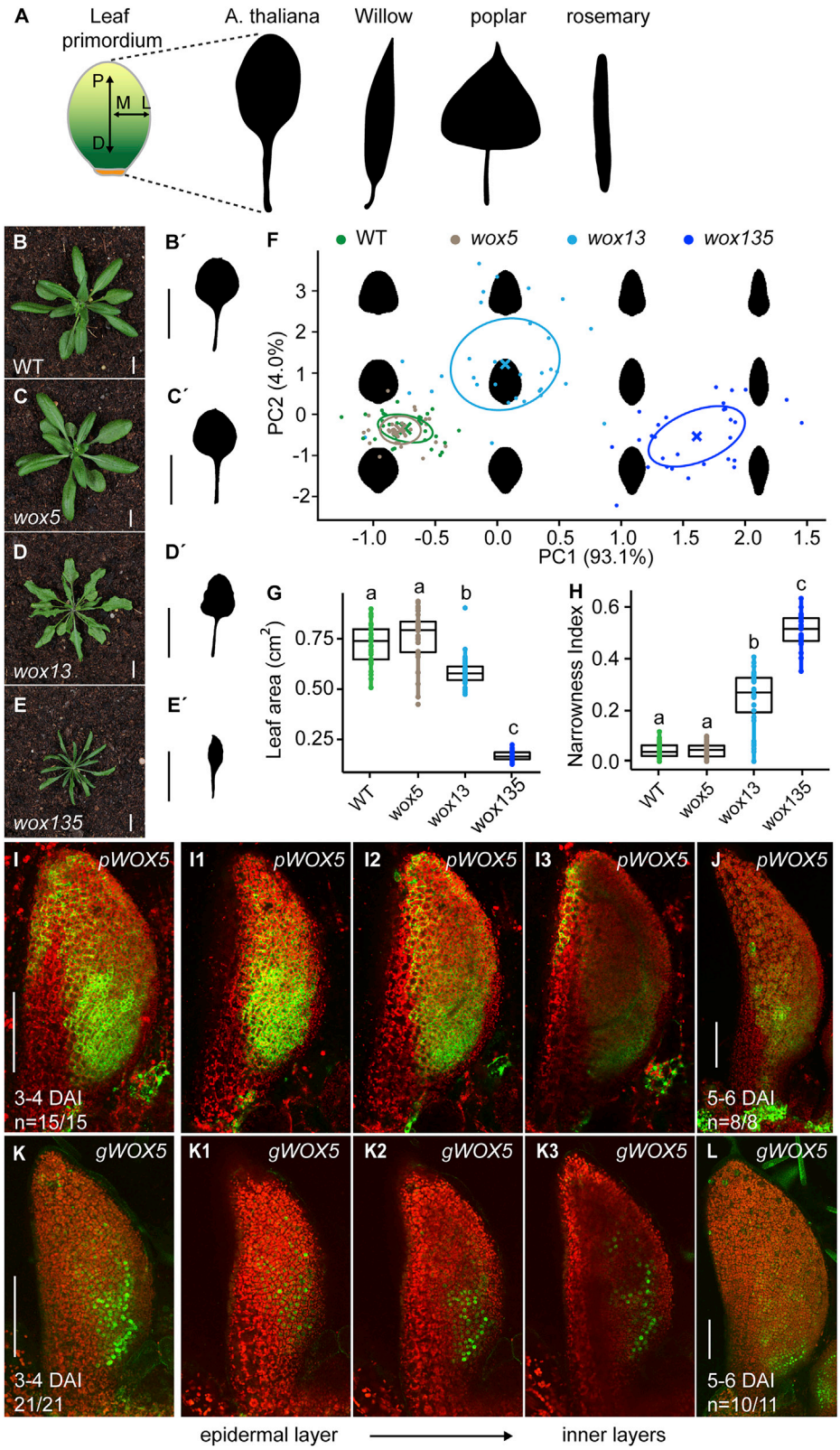

Figure 1. WOX5 Acts Redundantly with WOX1 and WOX3 to Regulate Leaf Lateral Growth

(A) Left: the growth gradient of a leaf primordium (green color), relative to the mediolateral (ML) and proximodistal (PD) axes. Right: leaf primordia can give rise to varied leaf shapes in different plant species.

(legend continued on next page)

(*PRS*/*WOX3*), regulate leaf blade outgrowth and marginal cell identity [8, 9, 10, 11]. The role of *WOX* genes in regulating leaf width appears to be broadly conserved among seed plants, as both monocot and eudicot loss-of-function *WOX* mutants display a narrow, strap-like leaf shape, indicative of aberrant lateral growth [8,9,11–14]. In *Arabidopsis*, *WOX1*/*WOX3* (*PRS*) have been proposed to promote lateral growth by influencing tissue identity [8]. Specifically, WOX action is thought to define a middle domain that contains the leaf margin in the growing leaf bud. This domain separates the abaxial and adaxial (dorsal and ventral) domains and regulates leaf blade outgrowth, downstream of adaxial/abaxial polarity [8]. However, how growth control contributes to this domain delimitation system is unknown. In addition, how WOX proteins regulate specific aspects of cellular growth in the leaf remains unclear. As such, we lack a clear understanding of how spatially distributed WOX action is translated into final leaf shape. During embryogenesis, WOX proteins promote SAM development by activating *HD-ZIP III* genes [15]. HD-ZIP IIIs promote adaxial leaf identity and are one of the key components of the adaxial/abaxial delimitation system postulated to interact with WOXs to promote lateral growth [8]. This raises the question as to whether such WOX-mediated *HD-ZIP III*-activation is also deployed post-embryonically to support lateral leaf expansion. In addition, findings obtained in *Medicago truncatula* (medicago) indicate that WOX proteins might influence auxin homeostasis [13]. However, how *WOX* genes affect auxin homeostasis, and whether alterations in auxin homeostasis cause *wox* mutant phenotypes, is not known. Additionally, there is evidence that auxin signaling may act upstream of *WOX* genes [16, 17], raising the possibility that feedbacks between auxin signaling and biosynthesis contribute to WOX function.

Here, we investigate the *WOX*-mediated control of leaf shape in *A. thaliana* and show that *WOX5* acts redundantly with *WOX1* and *WOX3* (*PRS*) to coordinate growth along the leaf PD and ML axes. We also show that *WOX1/3/5* genes affect lateral growth and organize a proximally focused growth distribution in the leaf blade that generates the characteristic ellipsoid shape of *A. thaliana* leaves. Furthermore, we show that this action depends in part on the localized WOX-mediated activation of YUCCA auxin biosynthetic gene expression. In conclusion, we identify a regulatory module that coordinates growth along perpendicular axes by defining the spatial distribution of a broadly acting growth hormone.

RESULTS

WOX5 Acts Redundantly with *WOX1* and *WOX3* to Regulate Leaf Shape

In various angiosperms, including medicago, petunia, and tobacco, single *wox1* or *wox3*/*prs* mutations cause an extremely narrow leaf phenotype [9, 13]. By contrast, *wox13* double mutants in *Arabidopsis* show only a moderate reduction in leaf width compared to wild type (WT) [8] (Figures 1B, 1B′, 1D, 1D′, and 1F–1H); this mild double-mutant phenotype suggests that considerable redundancy may exist among *WOX* genes in the *Arabidopsis* leaf. Consistent with this idea, we observed that loss of function of *WOX5* significantly enhanced the narrow leaf defect of the *wox13* double mutant (Figures 1B–1H, 1B′–1E′, and S1I). To investigate changes in leaf geometry in WOX single, double, and triple loss-of-function mutants, we used both univariate and multivariate shape analysis techniques (STAR Methods). This analysis showed that leaf size is reduced in *wox13* leaves and that leaf blades became narrower, with a more triangular leaf shape (Figures 1B, 1D, and 1F–1H). Loss of *WOX5* in *wox13* mutants led to a further reduction in leaf size and enhanced the narrow leaf defect throughout the whole leaf blade but did not significantly affect leaf shape in WT or single-mutant backgrounds (Figures 1B–1H and S1A–S1D). To understand where WOX5 is active in the leaf, we characterized the expression of a transcriptional (*pWOX5:GFP*) [18] and a genomic fusion reporter (*gWOX5-YFP*) [19] during early leaf development (Figures 1I–1L). We found that *pWOX5:GFP* is expressed in the entire leaf blade except for a region encompassing the leaf margin (Figures 1I–1I3), with higher expression in the regions of presumed vascular development (Figure 1I3). *pWOX5:GFP* expression forms a gradient that decreases toward the leaf tip (Figures 1I and 1J), although this expression is variable in the epidermis at later development stages (~5–6 days after initiation [DAI]; Figure 1J). *gWOX5-YFP* expression patterns in developing leaves are similar to those of the *pWOX5:GFP* transcriptional reporter line (Figures 1K and 1L), but expression is much weaker (STAR Methods). The expression of *pWOX5:GFP* and *gWOX5-YFP* also largely overlaps with that of *WOX1* and *WOX3* (*PRS*), except in regions near the leaf margin where *WOX1* and *WOX3* (*PRS*) are expressed but *WOX5* is not (Figures S1J–S1L) [8]. An overlap between *WOX1* and *WOX5* gene expression is also supported by *in situ* hybridization (ISH), in which we observed *WOX5* transcript to be localized in the "middle leaf domain," in a subdomain of that previously shown to be marked by *WOX1 mRNA* (Figure S1M) [8]. *WOX5* mRNA expression is stronger in distinct foci that correspond to the presumed developing vasculature, consistent with *gWOX5* expression that also marks developing vascular strands (Figure 1K3). The somewhat broader expression seen with *gWOX5* and particularly *pWOX5:GFP* relative to ISH may reflect differences in the capacity of the reporter genes to faithfully monitor *WOX5* gene expression or simply reduced sensitivity of ISH relative to confocal microscopy. Overall, these observations indicate that *WOX5* may act redundantly with *WOX1* and *WOX3* (*PRS*) in leaf development. This view is also

(B–E) Five-week-old *Arabidopsis* plants of the indicated genotypes; (B′)–(E′) show corresponding first leaf silhouettes.
(F) Leaf contour shape-space plot for the indicated genotypes, based on principal component analysis (PCA) (STAR Methods). PC1 and PC2 values for each contour (colored dots) are, respectively, plotted along the x and y axes as multiples of their respective standard deviations (% of explained variance is indicated). Crosses indicate genotype means; ellipses indicate half the standard deviation; $29 \leq n \leq 32$.
(G and H) Quantification of leaf blade area (G) and narrowness index (H) for the leaf contours in (F). The narrowness index is (1 − blade width/blade length). Letters a, b, and c in (G) and (H) indicate statistically significant groups (ANOVA followed by Tukey's test).
(I–L) Maximum projection confocal micrographs of transcriptional reporter *pWOX5:GFP* (*pWOX5*, I and J) and genomic fusion reporter *gWOX5-YFP* (*gWOX5*, K and L) in green and chloroplast auto-fluorescence in red. Note the similar expression patterns. (I1–K3) Sequential optical sections of confocal stacks of *pWOX5:GFP* (*pWOX5*, I1–I3) and *gWOX5-YFP* (*gWOX5*, K1–K3) signal, progressing from the epidermal to internal layers. The first pair of leaves was analyzed. Scale bars, 1 cm in (B)–(E) and (B′)–(E′); 100 μm in (I)–(L). See also Figure S1.

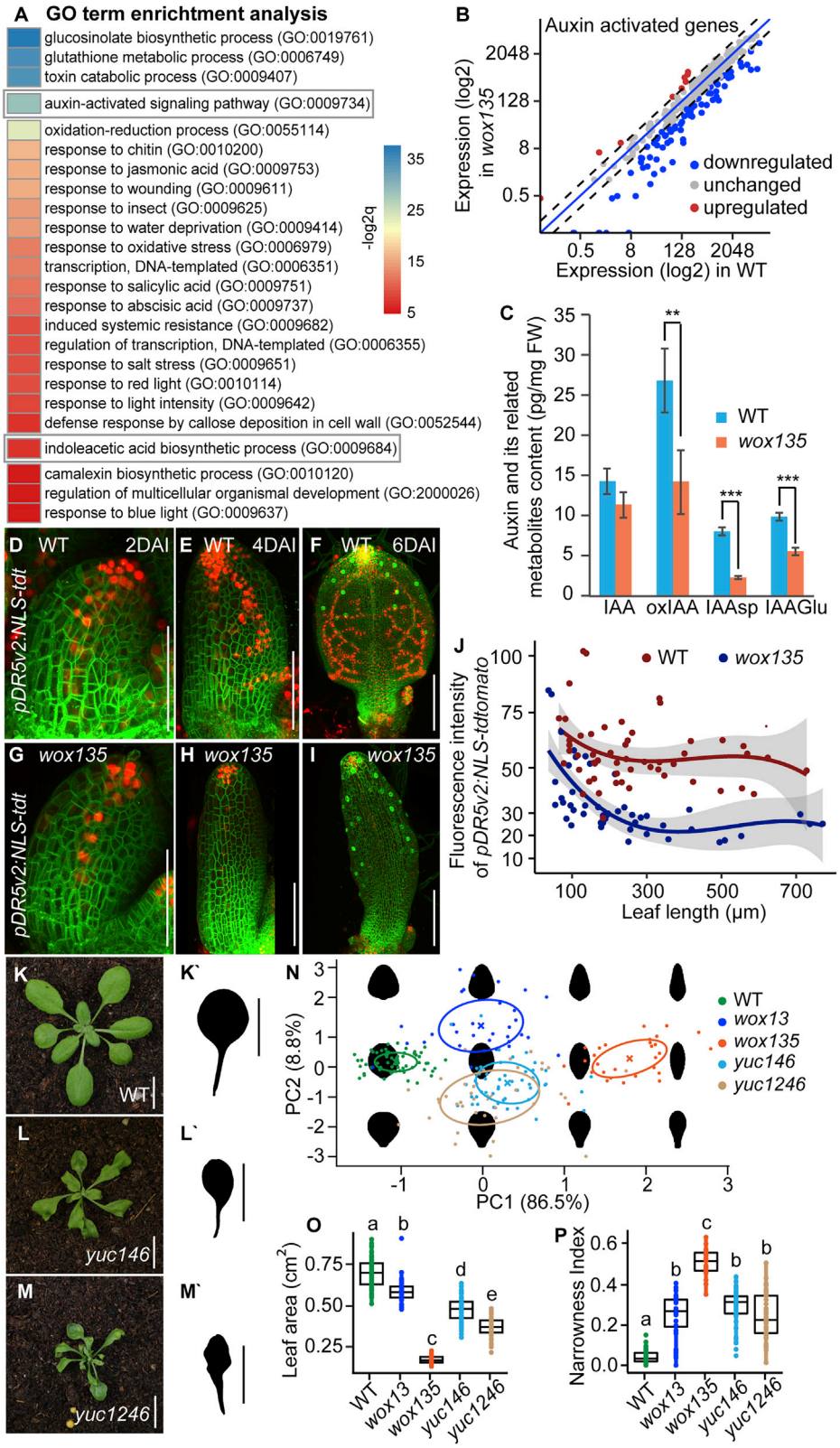

Figure 2. *WOX1*, *3*, and *5* Promote Auxin Biosynthesis

(A) GO term enrichment analysis of RNA sequence data shows that auxin-activated signaling pathways and biosynthetic processes are enriched among the genes downregulated in *wox135* mutants (GO terms enclosed in gray boxes).

(legend continued on next page)

consistent with previous findings that *WOX1*, *WOX3* (*PRS*), and *WOX5* can complement the narrow leaf defect of tobacco *LAM1* (*WOX1* ortholog) mutant [20]. Finally, we also observed that *pWOX5:GFP* expression expands to include this marginal region when it is expressed in *wox13* or *wox13wox5*/+ backgrounds (Figures S1N–S1Q). This effect likely contributes to the functional redundancy between *WOX1*, *3*, and *5*.

Next, we investigated whether *WOX* genes act during leaf development via the same molecular pathways employed during embryonic development. To this end, we tested whether HD-ZIP III mediates WOX1/3/5 function in the leaf, as in embryos [15], by expressing either a microRNA-insensitive version of *PHV* (*pWOX3:rPHV*) or a mimicry RNA against miR165/166 (*pWOX3:MIM165*) in the *wox135* mutant. In both cases, we found that increasing HD-ZIP III expression did not suppress the narrow leaf phenotype (Figures S1E–S1H). Although these findings do not preclude interactions between HD-ZIP III and WOX-dependent processes in developing leaf primordia [16], they suggest that, to shape leaf form, *WOX* genes act at least in part via different molecular pathways in the leaf and embryo.

WOX Genes Promote Auxin Synthesis in the Leaf

To investigate the molecular processes by which *WOX1*, *3*, and *5* regulate leaf shape, we performed RNA sequencing (RNA-seq) analysis of 6-day-old WT and *wox135* mutant seedlings. Compared to WT, 449 genes were upregulated (Table S1) and 778 genes were downregulated (Table S2) in *wox135* mutants (STAR Methods). Gene Ontology (GO) term enrichment analysis, performed using Panther Gene Ontology (STAR Methods), showed that auxin signaling pathways and auxin biosynthesis genes are highly enriched among the downregulated genes (Figure 2A), although no obviously enriched pathway/process was found among the upregulated genes. We compared a list of 335 auxin-induced transcripts [21] and all the *AUX/IAA* genes [22] (most of which are upregulated by auxin) against our deregulated gene list. This analysis showed that most of the auxin-induced and *AUX/IAA* genes are downregulated in the *wox135* mutant (Figures 2B and S2A). Consistent with our RNA-seq results, we found that the expression of the auxin activity reporter *pDR5v2:NLS-tdTomato* [23] was significantly reduced in mutant leaf primordia, coincident with the time that morphological defects first become apparent (Figures 2D–2J). Because auxin biosynthesis and signaling pathways are controlled via feedback loops [24], we reasoned that *WOX* genes might regulate growth by controlling auxin biosynthesis, which would then lead to changes in auxin responses. Consistent with this view, we measured auxin content of the *wox135* shoots (2 weeks old) via liquid chromatography-mass spectrometry. The lower levels of the IAA conjugates IAAsp and IAAGlu as well as the IAA catabolite oxIAA in *wox135* indicate that IAA biosynthesis is downregulated in this mutant (Figure 2C) [25]. Furthermore, the DR5 auxin reporter was upregulated by the *WOX3* (*PRS*) promoter-driven expression of the auxin biosynthesis gene *YUC1* (*pWOX3:YUC1*) in the *wox135* mutant (Figures S2B–S2I). These results support the hypothesis that WOX genes regulate auxin biosynthesis and indicate that auxin signaling is at least partly functional in the *wox135* mutant. To test whether *yucca* mutants display similar leaf development defects to those observed in multi-gene *wox* mutants, we analyzed leaf development in complex *yuc* mutants. We found that *yuc146* triple and *yuc1246* quadruple loss-of-function mutants develop narrower leaves, which partially mimic *wox13* and *wox135* mutant narrow leaf defects, albeit with more varied and asymmetric leaf shapes (Figures 2K–2P and 2K′–2M′). Taken together, these results suggest that auxin biosynthesis is impaired in *wox135* mutants and that WOXs and YUCCAs control leaf development partly via similar pathways.

To investigate the spatial-temporal expression of auxin biosynthetic genes during leaf development, we analyzed the expression of transcriptional reporter lines of *YUC1* (*pYUC1:3xNLS-GFP*; downregulated in our *wox135* RNA-seq data) and *YUC4* (*pYUC4:3xNLS-GFP*). Among the YUC family, YUC1 and YUC4 have previously been proposed to function in leaf shape [26]. Consistent with previous reports [26, 27], we found that, in WT plants, *pYUC1:3xNLS-GFP* is expressed in the marginal region of the leaf base (Figure 3A) and that *pYUC4:3xNLS-GFP* is strongly expressed at the tips of leaves and serrations from 2 to 4 DAI (Figure 3C). We also found that *pYUC4:3xNLS-GFP* is highly expressed in the marginal region of the leaf base (~2 DAI) and that this expression domain later expands distally along the margin (~3 DAI), eventually forming a gradient with the strongest expression at the leaf base (~4 DAI). By contrast, in *wox135* mutants, the expression of these reporters is strongly reduced in the marginal regions of the leaf, although expression of *YUC1* at the leaf petiole base and of *YUC4* at the leaf tip is maintained (Figures 3B and 3D). Thus, it appears that WOX genes are specifically required for expression of *YUC1* and *YUC4* at the leaf margin. To test whether *WOX* genes are also sufficient to upregulate *YUC1* and *YUC4* expression, we mis-expressed WOX3 (PRS) in both WT and mutant plants under the *RCO* (*REDUCED LEAF COMPLEXITY*) [28] promoter (*pRCO:WOX3*-mCherry). The *RCO* gene regulates leaf complexity in the Brassicaceae, and its promoter is active at the base of the leaf blade in a domain

(B) The expression levels of auxin-activated genes in WT and *wox135* from RNA-seq data.
(C) Free auxin and auxin metabolites levels in WT and *wox135* seedlings. $^{**}p < 0.01$ and $^{***}p < 0.001$ (t test; n = 4).
(D–I) Expression pattern of *pDR5v2:NLS-tdtomato* (red) in WT (D–F) and *wox135* (G–I) leaves at different DAI (day after initiation). Cells are outlined by a plasma membrane marker (green, *pUBQ10:acyl-YFP*).
(J) Quantification of *pDR5v2:NLS-tdtomato* expression during early development of leaves in WT (red dots, n = 56) and *wox135* (blue dots, n = 47). y axis is average pixel intensity per area in arbitrary unit (STAR Methods).
(K–M′) Three-week-old plants of the indicated genotypes, with corresponding leaf 1 silhouettes shown in (K′)–(M′).
(N) Leaf shape-space plot for leaf silhouettes of the indicated genotypes based on PCA (Figure 1F; STAR Methods); $29 \leq n \leq 48$.
(O and P) Quantification of the leaf blade area (O) and narrowness index (P; Figure 1H) for the data from (N). The letters a–e in (O) and (P) indicate statistically significant groups (ANOVA followed by Tukey's test).
Error bars in (C) represent SD. Scale bars, 50 μm in (D) and (G); 100 μm in (E) and (H); 200 μm in (F) and (I); 1 cm in (K)–(M) and (K′)–(M′). See also Figure S2 and Table S1 and S2.

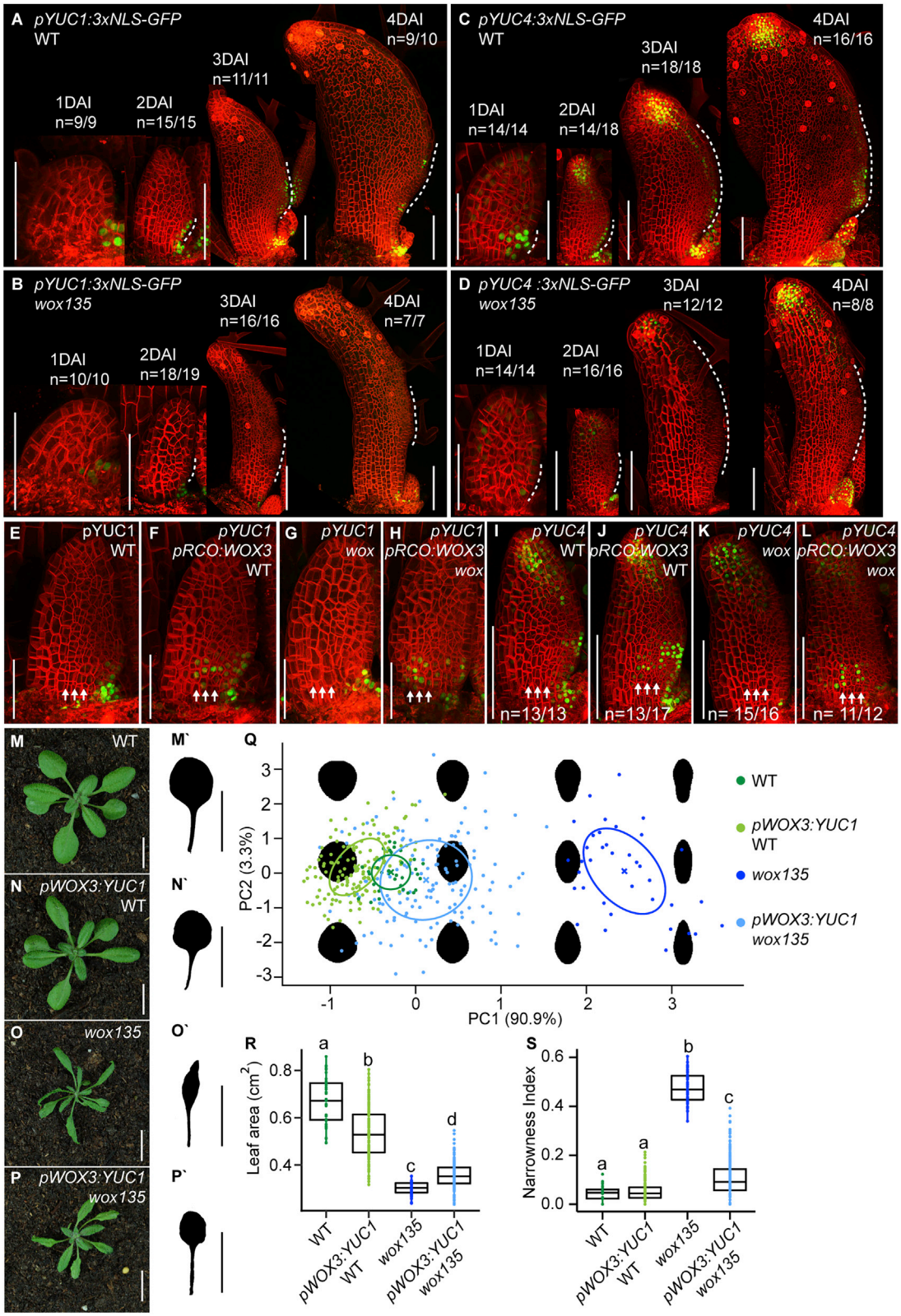

Figure 3. Auxin Partially Mediates WOX Function in Leaf Growth

(A–D) Expression pattern of *pYUC1:3xNLS-GFP* (*pYUC1*, green) and *pYUC4:3xNLS-GFP* (*pYUC4*, green) in WT (A and C) and *wox135* (B and D) leaf primordia (at different DAI, as indicated). Dashed lines in (A)–(D) highlight regions where GFP expression levels differ between WT and *wox135* primordia.

(legend continued on next page)

broader than the basal expression of both *YUC1* and *YUC4* (compare Figure S2J to Figures 3A and 3C). *RCO* expression is maintained in *wox135* mutant leaves, indicating that its expression is at least partially independent of *WOX* genes (Figure S2K). We found that *pRCO:WOX3-mCherry* ectopically induces *pYUC1:3xNLS-GFP* and *pYUC4:3xNLS-GFP* expression (Figures 3E–3L, S2L, and S2M–S2P, arrows), suggesting that *WOX3* (*PRS*) is sufficient to induce the expression of *YUC* genes. Taken together, we conclude that *WOX* genes positively regulate the transcription of *YUC* genes at the leaf margin during early leaf development.

Auxin Partially Mediates *WOX* Function in Lateral Leaf Growth

To investigate how the *WOX*-dependent activation of *YUC* genes regulates leaf shape, we expressed *YUC1* in the *wox135* mutant using the *WOX3* (*PRS*) promoter (*pWOX3:YUC1*). This promoter is active in the marginal regions of leaf primordia in both the WT and *wox135* mutants (*pWOX3:3xNLS-GFP* reporter shown in Figures S3A–S3F). *pWOX3:WOX3* rescues the leaf shape and area of *wox135* (Figures S3S–S3X). *pWOX3:YUC1* restores the narrow leaf shape of *wox135* to a rounder WT-like leaf shape (Figures 3M–3Q and 3S) and partially restores leaf size (Figure 3R). Notably, introducing *pWOX3:YUC1* into *wox135* mutants does not rescue the marginal defects of *wox135* mutants, because neither the adaxial marker *AS2* (*pAS2:3xNLS-GFP*) nor the margin-specific gene *LMI1* (*pLMI1:3xNLS-GFP*) [28, 29] were restored to their WT expression patterns by the expression of *pWOX3:YUC1* (Figures S3G–S3R). These results suggest that the shape of the leaf primordium is more sensitive to perturbations of WOX-mediated auxin biosynthesis than the delimitation of adaxial/abaxial and marginal domains, as respectively indicated by *AS2* and *LMI1* reporter gene expression, and that these two facets of WOX function are partly genetically separable. To address whether any auxin source in the leaf can mimic the local auxin synthesis that results from *WOX*-mediated *YUC* activation, we expressed *YUC1* in the *wox135* mutant using the epidermal layer-specific promoter *AtML1*, which is active in the meristem and leaf epidermis [30]. The *pAtML1:YUC1* transgene was not sufficient to suppress the *wox135* mutant narrow leaf shape (Figures S4A–S4G and S4A′–S4D′), indicating that development of the WT leaf blade does not simply depend on the accumulation of auxin in any location in the primordium. Thus, the local activation of *YUC* genes near the margin is important for leaf blade growth. The local requirement for *YUC* activity and auxin synthesis may also explain why the ubiquitous, exogenous application of auxin to medicago *stf* (*wox1*) plants did not rescue leaf shape [13].

WOX Genes Coordinate Leaf Growth by Locally Promoting Auxin Biosynthesis

We next sought to understand how WOX action shapes leaf form, which requires an understanding of how *WOX* genes affect organ-wide patterns of cellular growth. Although narrow-leaf *wox* mutant phenotypes are observed in many species [9, 13], such information is lacking, which prevents understanding how WOX proteins control leaf shape. To determine the cellular origin of the narrow leaf defect of *wox135* and ascertain how the *pWOX3:YUC1* transgene restores leaf shape when introduced into *wox135* mutant leaves, we performed time-lapse imaging of the WT, *wox135*, and *pWOX3:YUC1 wox135* lines. For each line, we imaged the first emerging true leaf from 2 DAI until 7 DAI (Figure S4H), when leaf shape divergence between genotypes becomes apparent. We constructed lineage maps from 2 DAI until 7 DAI (Figure S4I) and computed the key cell-level parameters that affect organ shape, including cell proliferation, cell growth, and cell area extension rates (Figures 4A–4I) using MorphoGraphX [31]. To connect cell-level parameters to tissue-level growth directions, we computed the growth of each clone with respect to an organ-wide coordinate system aligned with the PD and ML directions of the primordium at 2 DAI (Figure 4Q; STAR Methods). To identify the regional growth differences that underpin shape differences between our genotypes, we used growth alignment graphs, which allow cell growth at equivalent positions along the PD axis of leaf primordia to be compared (Figures 4J–4P and 4R; STAR Methods).

As WOX expression acquires a basally focused pattern of expression during leaf development (Figures 1I, 1K, S1N, and S1Q) [32], we reasoned that these genes may regulate the characteristic basipetal gradients of growth and proliferation (i.e., tip-to-base) observed in WT leaf blades [3, 4, 33]. To test this hypothesis, we examined the regional differences in growth and proliferation between WT and *wox135*. As expected, growth and cell proliferation had a basipetal gradient in WT leaves (Figures 4A, 4D, 4J, and 4K). However, in *wox135* leaf blades, proximal growth and proliferation were reduced, resulting in almost uniform rates of growth and proliferation along the PD axis (Figures 4B, 4E, 4J, and 4K). Likewise, the contribution of proximal cells at 2 DAI to leaf area and cell number at 7 DAI was reduced (Figures 4L and 4M). Thus, WOX activity affects leaf shape by promoting a basipetal distribution of growth and proliferation that is higher in the proximal blade.

Having found that WOX genes affect growth rates, we next sought to examine how WOX genes regulate growth directions by identifying how directional growth differs in *wox135* mutants compared to WT (Figures 4N–4P and 4R). To obtain tissue-aligned growth directions, we decomposed cell growth into directions aligned with the PD and ML axes of the primordium

(E–L) *pRCO:WOX3-mCherry* (*pRCO:WOX3*) induces *pYUC1:3xNLS-GFP* (*pYUC1*, green) and *pYUC4:3xNLS-GFP* (*pYUC4*, green) expression in both WT (E, F, I, and J) and *wox135* (G, H, K, and L) leaf primordia. Arrowheads highlight the region in which *pYUC1:3xNLS-GFP* and *pYUC4:3xNLS-GFP* (*pYUC4*) are ectopically induced by *pRCO:WOX3-mCherry*.

Cell membranes (A–L) are visualized using a plasma membrane marker (red, *pUBQ10:acyl-YFP*).

(M–P′) Four-week-old plants of the indicated genotypes (M–P) and their corresponding leaf 1 silhouettes (M′–P′).

(Q) Leaf shape-space plot for leaf silhouettes of indicated genotypes based on PCA (Figure 1F; STAR Methods); 14 T_2 transgenic families of each transgene were analyzed. $36 \leq n \leq 145$.

(R and S) Quantification of the leaf blade area (R) and narrowness index (S; Figure 1H) using the data from (Q). The letters a–d in (R) and (S) show statistically significant groups (ANOVA followed by Tukey's test).

Scale bars, 50 μm in 1 DAI of (A)–(D) and (E)–(H); 100 μm in the remaining panels of (A)–(D) and (I)–(L); 1 cm in (M)–(P′). See also Figures S2–S4.

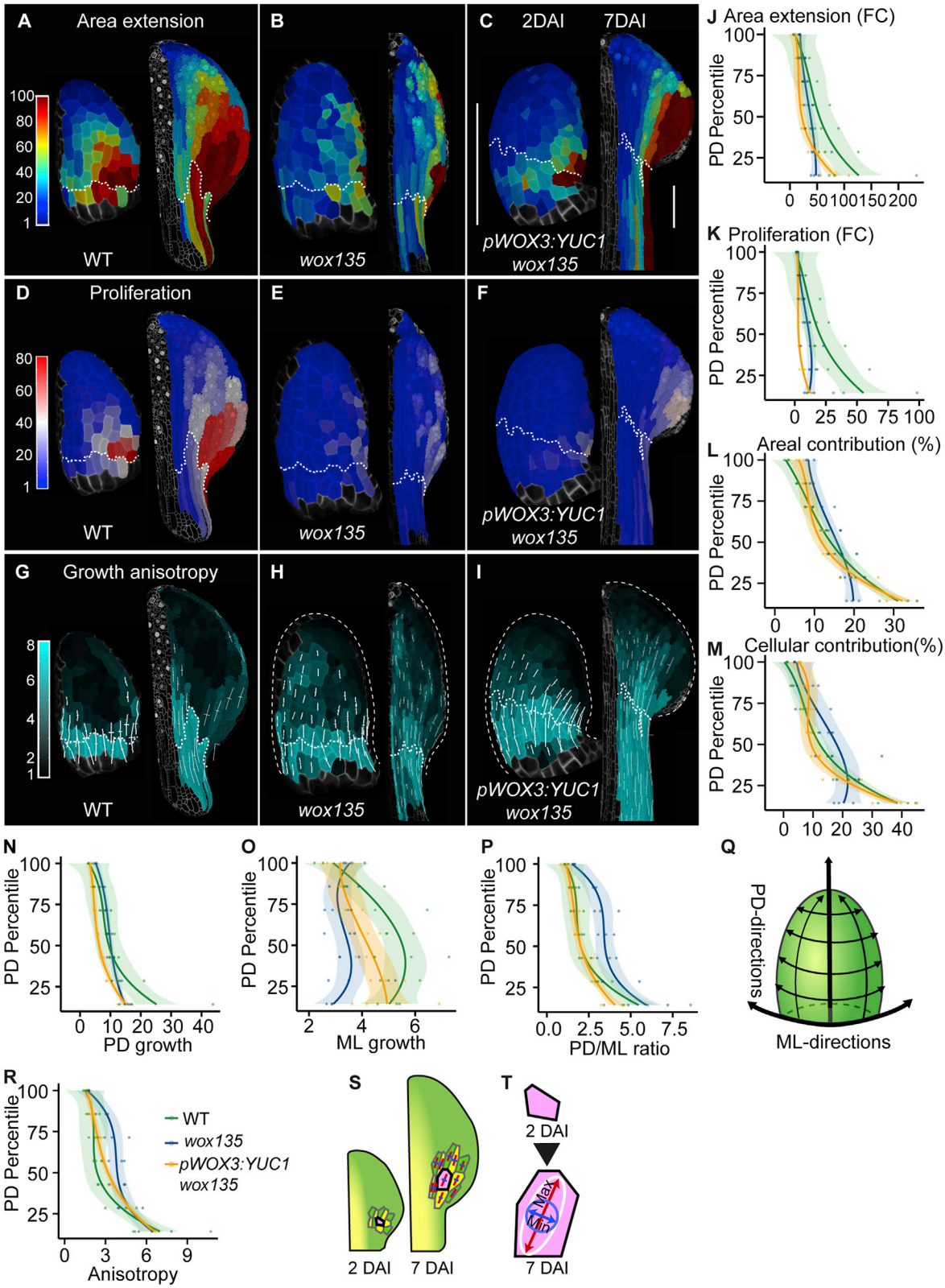

Figure 4. A Specific Spatial Pattern of Auxin Biosynthesis Is Required for Lateral Leaf Growth

(A–I) Heatmaps of area extension (A–C; fold change in area), cell proliferation (D–F; fold change in cell number), and growth anisotropy (G–I) for the indicated genotypes over 5 days growth, visualized on 2 DAI and 7 DAI leaf primordia. In (G)–(I), white lines indicate the direction of growth anisotropy for cells with

(legend continued on next page)

(Figure 4Q). The ratio of PD to ML growth (PD/ML growth ratio) indicates the relative preference for a region of the leaf blade to expand in length versus width. To quantify the degree to which clones grow with a preferred direction, independent of the tissue-aligned growth directions, we used the ratio of expansion rates in the max and min principal growth directions (anisotropy; Figures 4S and 4T) [31]. Combined with the PD/ML growth ratio, anisotropy provides a more comprehensive way to detect changes in growth direction between backgrounds. For example, a shift in growth direction from PD to ML will decrease the PD/ML growth ratio without necessarily affecting anisotropy. At the leaf blade base of *wox135* mutants, growth was anisotropic, similar to that of WT leaf blades (Figures 4G, 4H, and 4R), mirroring a reduction of growth in both tissue-aligned growth directions (with a slightly greater reduction in ML growth; Figures 4N–4P). By contrast, in the distal blade, anisotropy increased (Figures 4G, 4H, and 4R). Our quantifications indicate that, in the *wox135* mutant, ML growth was substantially reduced throughout most of the leaf blade (Figure 4O), although PD growth was unchanged in the distal leaf blade (Figure 4N), coinciding with increased anisotropy in this location. Together, these results indicate that *WOX* genes influence directional growth differently in different regions of the leaf blade in WT leaves: at the leaf blade base, they promote both lateral and PD growth, although lateral growth is promoted broadly in the leaf blade.

Having characterized the growth differences between WT and *wox135* mutants, we next sought to understand how *pWOX3:YUC1* suppresses the *wox135* mutant phenotype. Our analysis above (Figures 3Q and 3S) had shown that leaf shape is rescued in this background, producing a rounder leaf blade, but that leaf size is only slightly increased compared to *wox135* plants (Figure 3R). This observation suggests that, although *pWOX3:YUC1* only partially suppresses the growth phenotype of *wox135* leaves, it nevertheless rescues components of growth that are critical for leaf shape. To identify these components, we analyzed the growth of *pWOX3:YUC1 wox135* leaf blades and compared it to WT and *wox135* plants. Growth alignments show that *pWOX3:YUC1 wox135* leaf blades have a basipetal gradient of growth and proliferation, with this gradient being much less pronounced for proliferation (Figures 4C, 4F, 4J, and 4K). In this background, we observed an increase in the relative histogenic contribution of cells in the leaf base of 2 DAI to 7 DAI leaves compared to *wox135* leaves (Figures 4L, 4M, S4L, and S4M), shifting the corresponding growth alignments toward those of WT leaves. Thus, expressing *pWOX3:YUC1* in *wox135* plants rescues the basipetal gradient of leaf blade growth (Figures 4J and S4J) but does not restore absolute growth (Figures 4J, 4N, and 4O) or proliferation rates to WT levels (Figures 4D–4F, 4K, and S4K). In *pWOX3:YUC1 wox135* plants, area extension and proliferation were also reduced in the distal blade compared to *wox135* plants (Figures 4B, 4C, 4E, and 4F). Nonetheless, we observed increased area extension in the leaf blade base (Figures 4B, 4C, and 4J), which appeared to be the result of increased lateral growth (Figures 4N–4P and S4N–S4P; ML growth increased; PD growth decreased). This increase rescues the balance between PD and ML growth along the PD axis to WT levels (Figures 4P and S4P) and thus may explain the restoration of WT leaf shape in *pWOX3:YUC1 wox135* leaves.

Interestingly, although expressing YUC1 in the *pWOX3* domain reduces distal growth anisotropy toward WT levels, it did not change the growth anisotropy at the leaf blade base (Figure 4R). As such, our analysis of *pWOX3:YUC1 wox135* compared to *wox135* plants indicates that, although lateral growth is preferentially increased at the leaf blade base (Figure 4P), anisotropy in this region is largely unchanged. Together, these quantifications indicate a change in growth directions at the base of the leaf blade, which shifts from being closely aligned with the PD axis in *wox135* to take on a more lateral orientation in *pWOX3:YUC1* leaves (compare Figure 4H to Figure 4I).

Together, our results indicate that WOX-induced auxin biosynthesis shapes the basipetal gradient of leaf growth. Furthermore, they show that auxin biosynthesis in the WOX domain promotes growth laterally at the leaf base (Figure 4O) while reducing growth at the leaf tip (Figures 4B and 4C). This differential growth appears sufficient to restore the broad leaf shape of WT leaves in narrow-leafed *wox* triple mutants. Notably, our results suggest that the relative balance of lateral versus PD growth may be more important to leaf shape than absolute growth rates. Nonetheless, the inability of WOX-induced, auxin biosynthesis to rescue leaf size or distal leaf growth indicates that these components of leaf shape depend on additional pathways downstream of WOX.

anisotropy >3 (anisotropy is the ratio of max growth to min growth). Dashed lines indicate the leaf primordia outline in (H) and (I) and the division between blade and petiole in (A)–(I). Only clones from the blade were used for the analysis shown in (J)–(P) and (R).

(J–P) Alignment graphs of growth and proliferation for WT (green), *wox135* (blue), and *pWOX3:YUC1 wox135* (orange) leaf blades between 2 and 7 DAI. Cells were binned based on PD position at 2 DAI (y axis, percentile rank; n = 3 independent time-lapse experiments per background, 7 bins along the PD axis). Growth alignments of growth and proliferation (x axis, dependent variable) plotted as a function of PD position at 2 DAI (y axis, percentile rank) for mean cellular area extension (J), proliferation (K), relative areal (L), and cellular contribution (M), as well as PD growth (N), ML growth (O), and the ratio of PD to ML growth (P). Regression curves are cubic polynomials with 95% confidence intervals (shaded regions). FC in (J) and (K) designates fold change.

(Q) To derive tissue-aligned growth directions, a PD axis was ascertained at 2 DAI when primordia were approximately cylindrical. Using this axis, ML and PD directions were identified for each clone, providing a perpendicular coordinate system to quantify organ growth (STAR Methods).

(R) Growth alignment of anisotropy (x axis, dependent variable) plotted as a function of PD position at 2 DAI (y axis, percentile rank), as described for the growth alignments reported in (J)–(P).

(S and T) Quantifying clonal growth parameters in 2–7 DAI leaf primordia.

(S) Cells at 2 DAI are mapped to the corresponding daughter cells at 7 DAI, and the principal directions of growth (PDGs) (red and blue axes) are computed (shown for a basal region of the leaf blade).

(T) PDGs quantify the overall deformation of a clonal sector (visualized by the white ellipse) and indicate the directions and rates of minimum (min growth, blue) and maximum (max growth, red) expansion. The ratio of max to min growth indicates the degree to which clones expand in a preferred direction (anisotropy).

Scale bars in (C), applying to all images in (A)–(I), are 100 μm at 2 DAI and 200 μm in 7 DAI leaves. See also Figure S4.

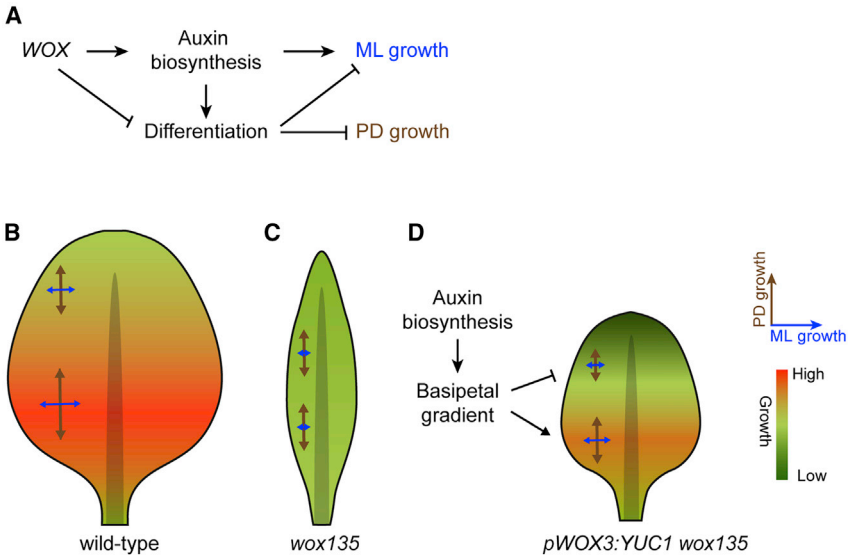

Figure 5. The Role of *WOX* Genes in Shaping Leaf Blade Form

(A) Conceptual model for the interactions between *WOX*, auxin biosynthesis, ML growth (blue), PD growth (brown), and differentiation during leaf blade development.

(B–D) Interpretation of WT, *wox135*, and *pWOX3:YUC1* leaf forms based on the model in (A).

(B) In WT leaves, *WOX* (1) promotes auxin biosynthesis (creating a broad leaf form) and (2) inhibits differentiation in the proximal blade. Delayed differentiation prolongs growth, increasing blade size.

(C) In *wox135* leaves, growth is uniform along the PD axis with little lateral growth.

(D) In *pWOX3:YUC1 wox135* leaves, auxin biosynthesis creates a basipetal growth gradient by (1) promoting lateral growth proximally and (2) inhibiting growth distally (by promoting differentiation). This changes the ratio of PD to ML growth to favor lateral growth, producing a broad leaf blade.

DISCUSSION

We have shown that *WOX1*, *3*, and *5* act redundantly to coordinate cellular growth, proliferation, and differentiation in the developing leaf primordium of *A. thaliana* (Figure 5). A single group of genes that control these processes might help to synchronize them during development to facilitate the emergence of leaves of the correct shape and size. We also provide evidence that auxin partially rescues basipetal growth in *wox1*, *3*, and *5* mutants by mediating two aspects of WOX action that contribute to the development of an elliptical leaf shape. Specifically, we propose that WOX-dependent auxin synthesis: (1) promotes lateral growth at the leaf blade base (Figures 4J and 4P) and (2) inhibits growth of the distal leaf blade, thus generating a basipetal gradient of growth (Figure 5D). Furthermore, our results show that the uniform provision of auxin biosynthetic gene expression in the leaf epidermis does not rescue the narrow leaf defects of *wox135*. This suggests that the precise spatial deployment of the WOX-auxin module is of crucial importance for leaf growth and form and complements the transport-based regulation of auxin distribution [34, 35]. Given that *pWOX3:YUC1* expression in *wox135* did not restore growth and proliferation to WT levels (Figures 4J and 4K), WOX genes must also act through pathways that are independent of auxin biosynthesis. This conclusion is also consistent with the fact that the leaf phenotype of *yuc* triple and quadruple mutants (Figures 2N and 2P) does not fully phenocopy the effects of *wox135* on leaf shape. Our observations indicate that *pWOX3:YUC1* expression also affects distal leaf blade development, where growth and proliferation were decreased in comparison to both WT and *wox135* mutants (Figures 4C, 4F, 4J, and 4K). Together, our findings show that WOX-dependent auxin production contributes to shaping cellular differentiation patterns in the leaf [3, 36]. As there is evidence that WOX expression is in turn influenced by auxin signaling, our results raise the possibility that a feedback between auxin activity and WOX action are an additional part of this module [16, 17].

In conclusion, we propose that *WOX* expression promotes a fast-growing, proliferative state and inhibits the action of differentiation-promoting compounds (including WOX-dependent auxin) in the proximal leaf blade. More distally, where WOX genes are not expressed, auxin would be free to promote differentiation. *WOXes* may thus contribute to the PD differentiation gradient observed in time-lapse data [3, 4] by inhibiting differentiation proximally in the blade and promoting it distally. Given that *WOXes* also promote lateral growth, we propose that these interactions contribute to the elliptical leaf shape of *A. thaliana* [1, 3, 4, 7]. This proposed role of the WOX/auxin module in shaping *Arabidopsis thaliana* leaf form can be conceptualized as a positional information system, with the following logic: an upstream regulator (WOX) promotes the synthesis of auxin, which serves as a long-range differentiation signal. This signal emanates from a basally localized growth zone within which the differentiation-inducing signal cannot act, allowing continued proliferation and growth. This basal dampening of differentiation promotes the continued activity of the growth zone despite the sustained production of the differentiation signal. As such, auxin may be one component of the distally acting morphogenetic signal that computational models predict is synthesized at the leaf base and regulates the basipetal progression of differentiation [7]. The expression of WOX proteins at the basal flanks of the developing leaf blade indicates that, in future work, it would be interesting to explore computational models that also incorporate morphogenetic signals originating from this domain.

Notably, our results with *pWOX3:YUC1* in *wox135* leaves also indicate that leaf shape can be restored to a shape very close to WT even if leaf size is only weakly rescued (Figures 1F and 1G). This observation suggests that the gradient of WOX-dependent leaf growth is at least as important for leaf shape as the absolute amount of growth. In this context, WOX/YUC-dependent lateral growth contributes to the increased width of the leaf blade compared to the petiole. The development of this aspect of leaf shape may involve an active change in growth directions owing to WOX/YUC-dependent changes in the polarity of cell growth [4, 37] or passive growth reorientation as a result of mechanical conflicts between the narrow petiole and the broader leaf blade [37, 38]. Distinguishing between these possibilities will require

study of WOX and YUC genetic mosaics combined with tissue-level mechanically informed models of leaf growth. Use of genetic mosaics and tissue-specific gene editing [39] will also help clarify the cell-specific functions of different *WOX* genes, as well as their interactions with *YUC* genes and the degree of their non-cell-autonomous function in the leaf blade [40]. Given the role of auxin in vascular development [41] and the likely interplay between vasculature pattern and leaf form [6, 13, 42], further investigation of WOX function in the vasculature will be of particular interest [43].

An implication of our findings is that evolutionary modifications of this WOX-YUC module (for example, modifications that change the domain of WOX expression, the degree of local differentiation inhibition, the efficiency of WOX-mediated *YUC* activation, or the rate of distal auxin transport) have the potential to contribute to the natural variation of leaf forms.

STAR★METHODS

Detailed methods are provided in the online version of this paper and include the following:

- KEY RESOURCES TABLE
- RESOURCE AVAILABILITY
  - Lead Contact
  - Material Availability
  - Data and Code Availability
- EXPERIMENTAL MODEL AND SUBJECT DETAILS
  - Plant material and growth conditions
- METHOD DETAILS
  - Plasmid construction
  - RNA *in situ* hybridization
  - RNA-seq
  - RNA-seq analysis
  - Fluorescence imaging
  - Growth tracking experiment
  - Leaf shape analysis
  - Growth Alignment Graphs
  - Auxin metabolite quantification
- QUANTIFICATION AND STATISTICAL ANALYSIS

SUPPLEMENTAL INFORMATION

Supplemental Information can be found online at https://doi.org/10.1016/j.cub.2020.09.037.

ACKNOWLEDGMENTS

We thank Prof. Thomas Laux for sharing a large number of materials used in this study. We thank Bjorn Pieper for discussions and advice on statistical modeling, R. Berndtgen for technical assistance, and Saiko Yoshida and Ziliang Hu for data validation. This work was supported by a Max Planck Society core grant to M.T., a Max Planck research fellowship to Z.Z., and a Marie Skłodowska-Curie IF (Horizon 2020, 703886) to A.R. K.L. and M.K. were supported by the Swedish research councils Formas, VR, and the Knut and Alice Wallenberg Foundation (KAW). We also thank the Swedish Metabolomics Center (SMC) (Umeå, Sweden) for access to instrumentation. M.T. also acknowledges support of the DFG Plant Morphodynamics Research Unit FOR2581.

AUTHOR CONTRIBUTIONS

Conceptualization, Z.Z. and M.T.; Methodology, Z.Z. and M.T.; Investigation, Z.Z., R.A.M., D.K., M.K., X.G., P.H., and K.L.; Software, A.R., B.H., and S.S.; Formal Analysis, A.R.; Writing – Original Draft, Z.Z., A.R., and M.T.; Writing – Review & Editing, Z.Z., A.R., and M.T.; Visualization, Z.Z. and M.T.; Resources, M.T.; Data Curation, M.T.; Supervision, M.T.; Project Administration, Z.Z. and M.T.; Funding Acquisition, M.T.

DECLARATION OF INTERESTS

The authors declare no competing interests.

Received: June 5, 2020
Revised: August 17, 2020
Accepted: September 11, 2020
Published: October 8, 2020

REFERENCES

1. Runions, A., and Tsiantis, M. (2017). The shape of things to come: from typology to predictive models for leaf diversity. Am. J. Bot. *104*, 1437–1441.
2. Zuniga, A. (2015). Next generation limb development and evolution: old questions, new perspectives. Development *142*, 3810–3820.
3. Kierzkowski, D., Runions, A., Vuolo, F., Strauss, S., Lymbouridou, R., Routier-Kierzkowska, A.-L., Wilson-Sánchez, D., Jenke, H., Galinha, C., Mosca, G., et al. (2019). A growth-based framework for leaf shape development and diversity. Cell *177*, 1405–1418.e17.
4. Kuchen, E.E., Fox, S., de Reuille, P.B., Kennaway, R., Bensmihen, S., Avondo, J., Calder, G.M., Southam, P., Robinson, S., Bangham, A., and Coen, E. (2012). Generation of leaf shape through early patterns of growth and tissue polarity. Science *335*, 1092–1096.
5. Whitewoods, C.D., Gonçalves, B., Cheng, J., Cui, M., Kennaway, R., Lee, K., Bushell, C., Yu, M., Piao, C., and Coen, E. (2020). Evolution of carnivorous traps from planar leaves through simple shifts in gene expression. Science *367*, 91–96.
6. Runions, A., Tsiantis, M., and Prusinkiewicz, P. (2017). A common developmental program can produce diverse leaf shapes. New Phytologist *216*, 401–418.
7. Fox, S., Southam, P., Pantin, F., Kennaway, R., Robinson, S., Castorina, G., Sánchez-Corrales, Y.E., Sablowski, R., Chan, J., Grieneisen, V., et al. (2018). Spatiotemporal coordination of cell division and growth during organ morphogenesis. PLoS Biol. *16*, e2005952.
8. Nakata, M., Matsumoto, N., Tsugeki, R., Rikirsch, E., Laux, T., and Okada, K. (2012). Roles of the middle domain-specific WUSCHEL-RELATED HOMEOBOX genes in early development of leaves in Arabidopsis. Plant Cell *24*, 519–535.
9. Vandenbussche, M., Horstman, A., Zethof, J., Koes, R., Rijpkema, A.S., and Gerats, T. (2009). Differential recruitment of WOX transcription factors for lateral development and organ fusion in Petunia and Arabidopsis. Plant Cell *21*, 2269–2283.
10. Zhao, F., Du, F., Oliveri, H., Zhou, L., Ali, O., Chen, W., et al. (2020). Microtubule-mediated wall anisotropy contributes to leaf blade flattening. Curr. Biol. Published online September 10, 2020. https://doi.org/10.1016/j.cub.2020.07.076.
11. Nardmann, J., Ji, J., Werr, W., and Scanlon, M.J. (2004). The maize duplicate genes narrow sheath1 and narrow sheath2 encode a conserved homeobox gene function in a lateral domain of shoot apical meristems. Development *131*, 2827–2839.
12. Scanlon, M.J., Schneeberger, R.G., and Freeling, M. (1996). The maize mutant narrow sheath fails to establish leaf margin identity in a meristematic domain. Development *122*, 1683–1691.
13. Tadege, M., Lin, H., Bedair, M., Berbel, A., Wen, J., Rojas, C.M., Niu, L., Tang, Y., Sumner, L., Ratet, P., et al. (2011). STENOFOLIA regulates blade outgrowth and leaf vascular patterning in Medicago truncatula and Nicotiana sylvestris. Plant Cell *23*, 2125–2142.
14. Cho, S.-H., Yoo, S.-C., Zhang, H., Pandeya, D., Koh, H.-J., Hwang, J.-Y., Kim, G.-T., and Paek, N.-C. (2013). The rice narrow leaf2 and narrow leaf3 loci encode WUSCHEL-related homeobox 3A (OsWOX3A) and function in

leaf, spikelet, tiller and lateral root development. New Phytol. *198*, 1071–1084.

15. Zhang, Z., Tucker, E., Hermann, M., and Laux, T. (2017). A molecular framework for the embryonic initiation of shoot meristem stem cells. Dev. Cell *40*, 264–277.e4.
16. Caggiano, M.P., Yu, X., Bhatia, N., Larsson, A., Ram, H., Ohno, C.K., Sappl, P., Meyerowitz, E.M., Jönsson, H., and Heisler, M.G. (2017). Cell type boundaries organize plant development. eLife *6*, e27421.
17. Guan, C., Wu, B., Yu, T., Wang, Q., Krogan, N.T., Liu, X., and Jiao, Y. (2017). Spatial auxin signaling controls leaf flattening in Arabidopsis. Curr. Biol. *27*, 2940–2950.e4.
18. Sarkar, A.K., Luijten, M., Miyashima, S., Lenhard, M., Hashimoto, T., Nakajima, K., Scheres, B., Heidstra, R., and Laux, T. (2007). Conserved factors regulate signalling in Arabidopsis thaliana shoot and root stem cell organizers. Nature *446*, 811–814.
19. Pi, L., Aichinger, E., van der Graaff, E., Llavata-Peris, C.I., Weijers, D., Hennig, L., Groot, E., and Laux, T. (2015). Organizer-derived WOX5 signal maintains root columella stem cells through chromatin-mediated repression of CDF4 expression. Dev. Cell *33*, 576–588.
20. Lin, H., Niu, L., McHale, N.A., Ohme-Takagi, M., Mysore, K.S., and Tadege, M. (2013). Evolutionarily conserved repressive activity of WOX proteins mediates leaf blade outgrowth and floral organ development in plants. Proc. Natl. Acad. Sci. USA *110*, 366–371.
21. Nemhauser, J.L., Mockler, T.C., and Chory, J. (2004). Interdependency of brassinosteroid and auxin signaling in Arabidopsis. PLoS Biol. *2*, E258.
22. Paponov, I.A., Paponov, M., Teale, W., Menges, M., Chakrabortee, S., Murray, J.A.H., and Palme, K. (2008). Comprehensive transcriptome analysis of auxin responses in Arabidopsis. Mol. Plant *1*, 321–337.
23. Liao, C.-Y., Smet, W., Brunoud, G., Yoshida, S., Vernoux, T., and Weijers, D. (2015). Reporters for sensitive and quantitative measurement of auxin response. Nat. Methods *12*, 207–210, 2, 210.
24. Weijers, D., and Wagner, D. (2016). Transcriptional responses to the auxin hormone. Annu. Rev. Plant Biol. *67*, 539–574.
25. Novák, O., Hényková, E., Sairanen, I., Kowalczyk, M., Pospíšil, T., and Ljung, K. (2012). Tissue-specific profiling of the Arabidopsis thaliana auxin metabolome. Plant J. *72*, 523–536.
26. Wang, W., Xu, B., Wang, H., Li, J., Huang, H., and Xu, L. (2011). YUCCA genes are expressed in response to leaf adaxial-abaxial juxtaposition and are required for leaf margin development. Plant Physiol. *157*, 1805–1819.
27. Cheng, Y., Dai, X., and Zhao, Y. (2007). Auxin synthesized by the YUCCA flavin monooxygenases is essential for embryogenesis and leaf formation in Arabidopsis. Plant Cell *19*, 2430–2439.
28. Vlad, D., Kierzkowski, D., Rast, M.I., Vuolo, F., Dello Ioio, R., Galinha, C., Gan, X., Hajheidari, M., Hay, A., Smith, R.S., et al. (2014). Leaf shape evolution through duplication, regulatory diversification, and loss of a homeobox gene. Science *343*, 780–783.
29. Vuolo, F., Mentink, R.A., Hajheidari, M., Bailey, C.D., Filatov, D.A., and Tsiantis, M. (2016). Coupled enhancer and coding sequence evolution of a homeobox gene shaped leaf diversity. Genes Dev. *30*, 2370–2375.
30. Takada, S., and Jürgens, G. (2007). Transcriptional regulation of epidermal cell fate in the Arabidopsis embryo. Development *134*, 1141–1150.
31. Barbier de Reuille, P., Routier-Kierzkowska, A.-L., Kierzkowski, D., Bassel, G.W., Schüpbach, T., Tauriello, G., Bajpai, N., Strauss, S., Weber, A., Kiss, A., et al. (2015). MorphoGraphX: a platform for quantifying morphogenesis in 4D. eLife *4*, 05864.
32. Alvarez, J.P., Furumizu, C., Efroni, I., Eshed, Y., and Bowman, J.L. (2016). Active suppression of a leaf meristem orchestrates determinate leaf growth. eLife *5*, e15023.
33. Donnelly, P.M., Bonetta, D., Tsukaya, H., Dengler, R.E., and Dengler, N.G. (1999). Cell cycling and cell enlargement in developing leaves of Arabidopsis. Dev. Biol. *215*, 407–419.
34. Zhao, Y. (2018). Essential roles of local auxin biosynthesis in plant development and in adaptation to environmental changes. Annu. Rev. Plant Biol. *69*, 417–435.
35. Brumos, J., Robles, L.M., Yun, J., Vu, T.C., Jackson, S., Alonso, J.M., and Stepanova, A.N. (2018). Local auxin biosynthesis is a key regulator of plant development. Dev. Cell *47*, 306–318.e5.
36. Challa, K.R., Rath, M., and Nath, U. (2019). The CIN-TCP transcription factors promote commitment to differentiation in Arabidopsis leaf pavement cells via both auxin-dependent and independent pathways. PLoS Genet. *15*, e1007988.
37. Kennaway, R., Coen, E., Green, A., and Bangham, A. (2011). Generation of diverse biological forms through combinatorial interactions between tissue polarity and growth. PLoS Comput. Biol. *7*, e1002071.
38. Verger, S., Long, Y., Boudaoud, A., and Hamant, O. (2018). A tension-adhesion feedback loop in plant epidermis. eLife *7*, e34460.
39. Decaestecker, W., Buono, R.A., Pfeiffer, M.L., Vangheluwe, N., Jourquin, J., Karimi, M., Van Isterdael, G., Beeckman, T., Nowack, M.K., and Jacobs, T.B. (2019). CRISPR-TSKO: a technique for efficient mutagenesis in specific cell types, tissues, or organs in Arabidopsis. Plant Cell *31*, 2868–2887.
40. Shimizu, R., Ji, J., Kelsey, E., Ohtsu, K., Schnable, P.S., and Scanlon, M.J. (2009). Tissue specificity and evolution of meristematic WOX3 function. Plant Physiol. *149*, 841–850.
41. Verna, C., Ravichandran, S.J., Sawchuk, M.G., Linh, N.M., and Scarpella, E. (2019). Coordination of tissue cell polarity by auxin transport and signaling. eLife *8*, e51061.
42. Scarpella, E., Barkoulas, M., and Tsiantis, M. (2010). Control of leaf and vein development by auxin. Cold Spring Harb Perspect Biol. *2*, a001511.
43. Ji, J., Strable, J., Shimizu, R., Koenig, D., Sinha, N., and Scanlon, M.J. (2010). WOX4 promotes procambial development. Plant Physiol. *152*, 1346–1356.
44. Robert, H.S., Grones, P., Stepanova, A.N., Robles, L.M., Lokerse, A.S., Alonso, J.M., Weijers, D., and Friml, J. (2013). Local auxin sources orient the apical-basal axis in Arabidopsis embryos. Curr. Biol. *23*, 2506–2512.
45. Yan, J., Gu, Y., Jia, X., Kang, W., Pan, S., Tang, X., Chen, X., and Tang, G. (2012). Effective small RNA destruction by the expression of a short tandem target mimic in Arabidopsis. Plant Cell *24*, 415–427.
46. Schindelin, J., Arganda-Carreras, I., Frise, E., Kaynig, V., Longair, M., Pietzsch, T., Preibisch, S., Rueden, C., Saalfeld, S., Schmid, B., et al. (2012). Fiji: an open-source platform for biological-image analysis. Nat. Methods *9*, 676–682.
47. Anders, S., and Huber, W. (2010). Differential expression analysis for sequence count data. Genome Biol. *11*, R106.
48. Mott, R., Yuan, W., Kaisaki, P., Gan, X., Cleak, J., Edwards, A., Baud, A., and Flint, J. (2014). The architecture of parent-of-origin effects in mice. Cell *156*, 332–342.
49. Kuhl, F.P., and Giardina, C.R. (1982). Elliptic Fourier features of a closed contour. Comput. Graph. Image Process. *18*, 236–258.
50. Kozlov, M.V., Wilsey, B.J., Koricheva, J., and Haukioja, E. (1996). Fluctuating asymmetry of birch leaves increases under pollution impact. J. Appl. Ecol. *33*, 1489–1495.
51. Chitwood, D.H., Headland, L.R., Ranjan, A., Martinez, C.C., Braybrook, S.A., Koenig, D.P., Kuhlemeier, C., Smith, R.S., and Sinha, N.R. (2012). Leaf asymmetry as a developmental constraint imposed by auxin-dependent phyllotactic patterning. Plant Cell *24*, 2318–2327.
52. Chitwood, D.H., Naylor, D.T., Thammapichai, P., Weeger, A.C., Headland, L.R., and Sinha, N.R. (2012). Conflict between intrinsic leaf asymmetry and phyllotaxis in the resupinate leaves of Alstroemeria psittacina. Front. Plant Sci. *3*, 182.
53. Hejnowicz, Z., and Romberger, J.A. (1984). Growth tensor of plant organs. J. Theor. Biol. *110*, 93–114.
54. Dumais, J., and Kwiatkowska, D. (2002). Analysis of surface growth in shoot apices. Plant J. *31*, 229–241.
55. Dobrev, P.I., and Kamínek, M. (2002). Fast and efficient separation of cytokinins from auxin and abscisic acid and their purification using mixed-mode solid-phase extraction. J. Chromatogr. A *950*, 21–29.

STAR★METHODS

KEY RESOURCES TABLE

REAGENT or RESOURCE	SOURCE	IDENTIFIER
Chemicals, Peptides, and Recombinant Proteins		
Propidium iodide (PI)	Sigma-Aldrich	87-51-4
Phusion Taq	Thermo Fisher	F553S
Plant Preservative Mixture (PPM)	Plant Cell Technology	250
XmaI	New England Biolabs	R0180M
BamHI	New England Biolabs	R3136T
BglII	New England Biolabs	R0144M
PstI	New England Biolabs	R0140M
NotI	New England Biolabs	R3189L
2,2′-Thiodiethanol	Sigma	166782-100G
Critical Commercial Assays		
CloneJET PCR Cloning Kit	Thermo Fisher Scientific	#K1231
RNeasy Plant Mini Kit	QIAGEN	#74904
SuperScript VILO cDNA Synthesis Kit	Invitrogen	#11755-050
Deposited Data		
RNA seq	This study	PRJEB38272
Experimental Models: Organisms/Strains		
A. thaliana: Columbia-0 (*Col-0*)	N/A	N/A
A. thaliana: wox1-101 (*wox1*)	[8]	N/A
A. thaliana: wox3-2 (*prs-2*)	[8]	N/A
A. thaliana: wox5-1 (*wox5*)	[18]	N/A
A. thaliana: wox1-101 wox3-2 (*wox13*)	[8]	N/A
A. thaliana: wox1-101 wox5-1 (*wox15*)	This study	N/A
A. thaliana: wox3-2 wox5-1 (*wox35*)	This study	N/A
A. thaliana: wox1-101 wox3-2 wox5-1 (*wox135*)	This study	N/A
A. thaliana: pWOX5:GFP	Gift from Thomas Laux	N/A
A. thaliana: pWOX3:rPHV x wox135	This study	N/A
A. thaliana: pWOX3:MIM165/166 x wox135	This study	N/A
A. thaliana: pDR5v2:NLS-tdtomato x pUBQ10:acyl-YFP	This study	N/A
A. thaliana: pDR5v2:NLS-tdtomato x pWOX3:YUC1 x pUBQ10:acyl-YFP	This study	N/A
A. thaliana: pDR5v2:NLS-tdtomato x wox135 x pUBQ10:acyl-YFP	This study	N/A
A. thaliana: pDR5v2:NLS-tdtomato x pWOX3:YUC1 x wox135 x pUBQ10:acyl-YFP	This study	N/A
A. thaliana: yuc146	[27]	N/A
A. thaliana: yuc1246	[27]	N/A
A. thaliana: pRCO:3xNLS-GFP x pUBQ10:acyl-YFP	This study	N/A
A. thaliana: pRCO:3xNLS-GFP x wox135 x pUBQ10:acyl-YFP	This study	N/A
A. thaliana: pYUC1:3xNLS-GFP x pUBQ10:acyl-YFP	This study	N/A

(*Continued on next page*)

Continued

REAGENT or RESOURCE	SOURCE	IDENTIFIER
A. thaliana: pYUC1:3xNLS-GFP x pUBQ10:acyl-YFP x pRCO:WOX3-mcherry	This study	N/A
A. thaliana: pYUC1:3xNLS-GFP x wox135 x pUBQ10:acyl-YFP	This study	N/A
A. thaliana: pYUC1:3xNLS-GFP x wox135 x pUBQ10:acyl-YFP x pRCO:WOX3-mcherry	This study	N/A
A. thaliana: pYUC4:3xNLS-GFP x pUBQ10:acyl-YFP	This study	N/A
A. thaliana: pYUC4:3xNLS-GFP x pUBQ10:acyl-YFP x pRCO:WOX3-mcherry	This study	N/A
A. thaliana: pYUC4:3xNLS-GFP x wox135 x pUBQ10:acyl-YFP	This study	N/A
A. thaliana: pYUC4:3xNLS-GFP x wox135 x pUBQ10:acyl-YFP x pRCO:WOX3-mcherry	This study	N/A
A. thaliana: pUBQ10:acyl-YFP	This study	N/A
A. thaliana: pWOX3:YUC1 x pUBQ10:acyl-YFP	This study	N/A
A. thaliana: wox135 x pUBQ10:acyl-YFP	This study	N/A
A. thaliana: pWOX3:YUC1 x wox135 x pUBQ10:acyl-YFP	This study	N/A
A. thaliana: pWOX3:3xNLS-GFP	This study	N/A
A. thaliana: pWOX3:3xNLS-GFP x wox135	This study	N/A
A. thaliana: pLMI1:3xNLS-GFP x pUBQ10:acyl-YFP	This study	N/A
A. thaliana: pLMI1:3xNLS-GFP x pWOX3:YUC1 x pUBQ10:acyl-YFP	This study	N/A
A. thaliana: pLMI1:3xNLS-GFP x wox135 x pUBQ10:acyl-YFP	This study	N/A
A. thaliana: pLMI1:3xNLS-GFP x wox135 x pWOX3:YUC1 x pUBQ10:acyl-YFP	This study	N/A
A. thaliana: pAS2:3xNLS-GFP x pUBQ10:acyl-YFP	This study	N/A
A. thaliana: pAS2:3xNLS-GFP x pWOX3:YUC1 x pUBQ10:acyl-YFP	This study	N/A
A. thaliana: pAS2:3xNLS-GFP x wox135 x pUBQ10:acyl-YFP	This study	N/A
A. thaliana: pAS2:3xNLS-GFP x wox135 x pWOX3:YUC1 x pUBQ10:acyl-YFP	This study	N/A
A. thaliana: pAtML1:YUC1 x wox135 x pUBQ10:acyl-YFP	This study	N/A
A. thaliana: pAtML1:YUC1 x pUBQ10:acyl-YFP	This study	N/A
A. thaliana: pWOX3:WOX3-GFP	This study	N/A
A. thaliana: pWOX3:WOX3-GFP x wox135	This study	N/A
Oligonucleotides		
All the oligonucleotides	This study	Table S3
Recombinant DNA		
pWOX3:rPHV	This study	N/A
pWOX3:MIM165/166	This study	N/A
pWOX3:WOX3-GFP	This study	N/A
pDR5v2:NLS-tdtomato	This study	N/A
pWOX3:YUC1	This study	N/A

(*Continued on next page*)

Continued

REAGENT or RESOURCE	SOURCE	IDENTIFIER
pRCO:WOX3-mCherry	This study	N/A
pRCO:3xNLS-GFP	This study	N/A
pYUC1:3xNLS-GFP	[44]	N/A
pYUC4:3xNLS-GFP	This study	N/A
pWOX3:3xNLS-GFP	This study	N/A
pLMI1:3xNLS-GFP	This study	N/A
pAS2:3xNLS-GFP	This study	N/A
pAtML1:YUC1	This study	N/A
Software and Algorithms		
LeafI (python)	This study	https://gitlab.mpcdf.mpg.de/g-adamrunions/leafinterrogator_zhang_et_al
MorphoGraphX	[31]	http://www.mpipz.mpg.de/MorphoGraphX/

RESOURCE AVAILABILITY

Lead Contact

Further information and requests for resources and reagents should be directed to and will be fulfilled by the Lead Contact Miltos Tsiantis (tsiantis@mpipz.mpg.de).

Material Availability

Plasmids and seed generated in this study have been deposited in relevant collections of the Tsiantis lab in the Max Planck Institute for Plant Breeding Research and will be distributed upon request. Newly generated material is outlined in the Key Resources Table.

Data and Code Availability

The accession number for the RNA-seq reported in this paper is European Nucleotide Archive (ENA): PRJEB38272.

The deregulated genes are listed in Tables S1 and S2.

The LeafI software and data used to perform leaf shape analysis is available from https://gitlab.mpcdf.mpg.de/g-adamrunions/leafinterrogator_zhang_et_al.

The R-Scripts and data used to perform growth alignments are available from https://gitlab.mpcdf.mpg.de/g-adamrunions/growthanalysisscript_zhang_et_al.

EXPERIMENTAL MODEL AND SUBJECT DETAILS

Plant material and growth conditions

All transgenic plants and mutants were in *Arabidopsis thaliana* Col-0 background and listed in Key Resources Table. Plants were grown on soil in a growth chamber under long day conditions (16 h/8h light/dark, 110 $\mu Em^{-2}s^{-1}$) at 20 ± 2°C, with 65 ± 10% relative humidity. For time-lapse experiments, soil-grown plants were transferred 1 day after germination to half MS medium supplemented with 1% sucrose, 0.1% PPM and grown in long day conditions described above.

METHOD DETAILS

Plasmid construction

All constructs were generated with conventional restriction enzyme digestion and ligation (Key Resources Table). Newly amplified sequences were confirmed by sequencing. Primers used are listed in Table S3. *WOX3* promoter (*pWOX3*) was amplified and ligated to the commercial plasmid pJet1.2 from CloneJET PCR Cloning Kit. *pWOX3* was excised by XmaI and ligated to pBJ36 intermediate vector. For *pWOX3:rPHV*, *rPHV* fragment was excised from *pWOX2:rPHV* by *BamH*I [15] and ligated to pBJ36 after the *WOX3* promoter. For *pWOX3:MIM165/166*, *MIM165/166* fragment was excised from *MIM165/166* in pJet [45] by BglII and ligated to pBJ36 after the *WOX3* promoter. For *pWOX3:WOX3-GFP*, *WOX3-GFP* was synthesized and ligated in pUC57. *WOX3-GFP* was excised by BglII and ligated to pBJ36 after the *WOX3* promoter. For *pWOX3:YUC1*, *YUC1* coding sequence was amplified and ligated to pJet1.2. *YUC1* was excised by *BamH*I and ligated to pBJ36 after the *WOX3* promoter. All these intermediate constructs were digested by *Not*I to obtain the targeted fragments and ligated to binary vector pMLBart. pMLBart gives Spectinomycin resistance in bacteria and Basta resistance in plants.

For *pRCO:WOX3-mCherry*, *WOX3* coding sequence without stop codon was amplified and ligated together with *mCherry* in pJet1.2. *WOX3-mCherry* was excised by *BamH*I and BglII and ligated to pBJ36 after *pRCO* [28]. *pRCO:WOX3-mCherry* was excised by *Not*I and ligated to pGreenII.

For *pYUC4:3xNLS-GFP* and *pAS2:3xNLS-GFP*, *YUC4* promoter (*pYUC4*) and *AS2* promoter (*pAS2*) were amplified and ligated to pJet1.2. *pYUC4* and *pAS2* were excised by XmaI and ligated to pBJ36 before *3xNLS-GFP*. *pYUC4:3xNLS-GFP* and *pAS2:3xNLS-GFP* was excised by *Not*I and ligated to binary vector pMLBart.

For *pWOX3:3xNLS-GFP*, *pWOX3* was excised from *pWOX3* in pJet1.2 and ligated to *3xNLS-GFP* in pGreenII. For *pRCO:3xNLS-GFP*, *pRCO* was excised from pBJ36 by PstI and *BamH*I and ligated to *3xNLS-GFP* in pGreenII. For *pLMI1:3xNLS-GFP*, *LMI1* promoter (*pLMI1*) was amplified and ligated to pBJ36. *pLMI1* was excised by SalI and XmaI and ligated to *3xNLS-GFP* in pGreenII. All these plasmids give Kanamycin resistance in bacteria and Methotrexate resistance *in planta*.

For *DR5v2:NLS-tdtomato* which was aimed to change plant resistance, *DR5v2:tdtomato* was excised from pGreenII by SalI and *Not*I (Kanamycin resistance *in planta* [23],) and ligated to pGreenII (Norfloxacin resistance *in planta*).

For *pAtML1:YUC1*, *YUC1* coding sequence was excised out using *BamH*I from *YUC1* in pJet1.2 [15] and ligated to pGreenII after the *AtML1* promoter. This confers Kanamycin resistance in bacteria and Methotrexate resistance *in planta*.

Plant transformations were performed using *Agrobacterium tumefaciens* strain GV3101 and the floral dipping method. All the transgenic plants were genotyped in the T1 generation for transgenes and/or mutant background. Plants carrying two transgenes or different mutant genotypes were produced by crossing and analyzed in the F1 generation.

For Figure S1G, 8 out of 8 independent transgenic lines displayed the phenotypes as shown in Figure S1G. For Figure S1H, 13 out of 13 independent transgenic lines displayed the phenotypes as shown in Figure S1H. For Figures 3Q–3S, 13 T2 families were analyzed for both *pWOX3:YUC1* in wild-type and *wox135*. For Figures S3S and S3T, the first pair of leaves from 6 T2 transgenic families of *pWOX3:WOX3* in wild-type and in *wox135*, respectively, were analyzed. For Figures S4E–S4G, the first pair of leaves from 11 and 17 T1 transgenic plants of *pAtML1:YUC1* in wild-type and in *wox135*, respectively, were analyzed.

RNA *in situ* hybridization

RNA *in situ* hybridizations on 8 μm sections through fixed and paraffin-embedded shoot apices of 2- to 3-wk-old short-day grown *A. thaliana* Col-0 plants were performed largely as previously described [28]. Digoxigenin-labeled antisense RNA probes to *A. thaliana WOX5* (AT3G11260) were generated using a synthetic DNA template with the T7 RNA polymerase-binding sequence motif, 5′-CCCTATAGTGAGTCGTATTACGCAC-3′, added to its 3′ end (synthesized by BioCat GmbH, Heidelberg, Germany). The template represented positions 309-883 (5′-ACGAC .... ATTGA-3′) of NCBI Reference Sequence NM_111961.4. After hybridization and washing, the sections were covered with 70% TDE at pH = 9 and imaged with a Zeiss Axio Imager equipped with a digital color camera and DIC optics. To cover a broader hybridization pattern, three consecutive sections were registered and minimum projections were generated using the image processing package Fiji [46].

RNA-seq

6-day-old seedlings of wild-type and *wox135* mutant on half MS medium were treated with Dexamethasone (10μM) for 4 hours. The cotyledons, root and half of the hypocotyl of seedlings were removed, and the remaining part including the leaves and ~2mm hypocotyl were collected. In total, 3 replicates for WT and *wox135* (1 *wox135* replicate failed in later RNA-seq analysis, therefore 2 replicates were left for transcriptome analysis) were prepared and total RNA was isolated using plant mini RNeasy kit (QIAGEN) for sequencing.

Library preparation and sequencing have been performed at the Max Planck Genome Center Cologne, Germany (https://mpgc.mpipz.mpg.de/home/). 700 ng total RNA has initially been used for polyA enrichment with the NEBNext Poly(A) mRNA Magnetic Isolation Module (New England Biolabs). Subsequent library preparation has been performed with NEBNext Ultra Directional RNA Library Prep Kit for Illumina (New England Biolabs) according to the manufacturer's instructions. Quality and quantity were assessed at all steps via capillary electrophoresis (TapeStation, Agilent Technologies) and fluorometry (Qubit, Thermo Fisher Scientific). Libraries were immobilized and processed onto a flow cell with cBot (Illumina) and subsequently sequenced on HiSeq2500 system (Illumina) with 2 × 100 bp paired end reads.

RNA-seq analysis

Paired-end reads were aligned to the reference genome TAIR10 for *A. thaliana* using TopHat2 (1) with parameters "–max-multihits 10–coverage-search–microexon-search–mate-std-dev 40–library-type fr-secondstrand–max-intron-length 30000." Raw read counts per gene were quantified with HTSeq v0.5.4p1 (http://www-huber.embl.de/users/anders/HTSeq/) using the " -t CDS -s reverse" option. Differential expression between samples from the same species was determined using DESeq [47]. We found the most sensitive parameter settings for the function estimateDispersions were method = "blind," and sharingMode = "fit-only" [48]. The cutoff of deregulated genes is fold change > 1.5 and adjusted $p < 0.05$. GO term enrichment was analyzed via Panther Geneontology (http: //pantherdb.org/webservices/ go/overrep.jsp).

Fluorescence imaging

We used a SP8 upright confocal microscope equipped with a long working-distance water immersion objective (AP 20x/0.8 or AP 40x/0.8; Leica) to perform all imaging analyses. Excitation wavelengths for different fluorescence markers were as following: an argon laser with 488 nm for GFP, 514 nm for VENUS and YFP, and 561nm for tdTomato. Images in a set of experiments which needed to be

compared among each other were collected under the same settings. Chlorophyll autofluorescence was detected by excitation at 633 nm using a HeNe laser with 639-706 nm bandpass filter. For *pWOX5:GFP* and *gWOX5-YFP* (Figures 1I–1L), stronger laser power was used for the *gWOX5-YFP* reporter to detect the signal. The bandpass filter for *pWOX5:GFP* was 493-560 nm and 521-582 nm for *gWOX5-YFP*. Images were processed using LasX (Leica) analyzed using ImageJ or MorphGraphX software [31], and visualized by Photoshop (Adobe). For *pDR5v2:NLS-tdtomato*, leaf 1 to leaf 6 were taken for imaging. Signal intensity of *pDR5v2:NLS-tdtomato* was quantified via ImageJ using the cumulative signals from all the Z stacks of one leaf which were imaged under identical conditions.

Growth tracking experiment

After 1 day of germination, cotyledons of plants were carefully dissected out. Time-lapse imaging and analysis was performed according to the method described in [3]. Imaging was performed at 24h intervals, but at the last time point this interval was ~36h. Independent images were acquired at the indicated time-points.

Leaf shape analysis

To obtain leaf silhouettes and to quantify leaf shape, the first pair of leaves of 3-weeks-old plants were collected, flattened onto transparent adhesive paper, and scanned to obtain images. Leaf silhouettes were analyzed using Leaf Interrogator (LeafI), a GUI-based system providing an integrated pipeline for leaf shape analysis. LeafI is implemented in Python3.5, with a PyQt5 based GUI. LeafI was used to (1) extract leaf contours from images, (2) process contours to extract the leaf blade, (3) calculate simple shape measures (Figures 1G, 1H, 2O, 2P, 3R, 3S, S3T, S4F, and S4G), and (4) perform shape-space analysis and visualization (Figures 1F, 2N, 3Q, S3S, and S4E). Additional details are provided below.

1. Contour extraction: Image processing for the purpose of contour extraction was performed using OpenCV (V. 3.2.0.7). Binary thresholding was used to separate leaves from the image background, and a vector contour was extracted for each leaf (e.g., a sequence of 2D positions).
2. Contour processing: Contours were edited to delete the petiole and specify 2 common landmarks (the tip and base of the leaf-blade). The point of blade-petiole separation was identified manually by determining the point where the petiole begins to widen. Blade contours were resampled to obtain 60 points (semi-landmarks) on the contour intervals connecting the two-landmarks, yielding 122 points per contour (60 points on the left margin, 60 points on the right margin, and 2 landmarks). The 60 points were placed using an arc-length sampling of the contour (i.e., sample points were placed at equidistant points along each contour interval).
3. Simple shape measures: The resampled contours were used to compute the area and narrowness index for each blade. The narrowness index (also called *elongation*) is calculated from the minimum area rectangle enclosing the contour by taking the ratio of the rectangle's dimensions:

$$narrowness\ \ index\ \ = 1 - width/length. (\text{with length} \geq \text{width})$$

Areas and narrowness indices were exported from LeafI as csv files, and plotted in R. Areas in LeafI are reported in pixels^2 and were converted to cm^2 based on image dimensions.

4. Shape space analysis and visualization: Shape spaces visualize symmetric variation in leaf blade shape (Figures 1F, 2N, 3Q, S3S, and S4E), and were obtained by performing Elliptical Fourier Descriptor (EFD) analysis on the resampled leaf blade contours [49]. Using symmetric variation eliminates asymmetric variation resulting from confounding factors including: environment and developmental noise (i.e., fluctuating asymmetry [50]), chirality of phyllotaxy [51], and variable phenotypes that obscured the overall shape of the blade (e.g., *yuc126*, *yuc1246* mutants). Normalized EFDs were used for this analysis, as these provide a translation, rotation and scale invariant representation of the leaf contours. Rotation invariant coefficients were obtained by rotating contours to align the landmarks (leaf tip and leaf base) with the y axis before EFDs were computed [52]. Translation and scale-invariant EFDs were calculated as described in Kuhl and Giardina [49]. Principle Component Analysis was performed on the first 64 harmonics of the Fourier coefficients. To analyze symmetrical aspects of blade shape, Fourier coefficients capturing asymmetric variation about the main axis of the leaf (i.e., the line connecting the leaf tip and base) were set to zero prior to performing PCA [52]. The plots in Figures 1F, 2N, 3Q, S3S, and S4E were created using the Matplotlib library (V 2.0), and plotting the PCA values for the first two principal components. The first two components account for more than 94% of variance in all cases, indicating that they capture the majority of the symmetric shape variation of the leaf blade. Ellipses indicate half a standard deviation of the mean for each group, computed from the eigen-decomposition of the covariance matrix for that group.

Growth Alignment Graphs

To analyze the distribution of growth and proliferation in the blades of leaf primordium in *A. thaliana* wild-type, *wox135* and *pWOX3:-YUC1 wox135* plants between 2-7 DAI, we used growth alignment graphs [3]. Growth alignment graphs provide a method to compare equivalent regions along the Proximal-Distal axis (PD-axis) of leaf primordia in different backgrounds. Information on each clone was computed in MorphoGraphX [31], and exported as a csv file. This data was used to generate growth alignment graphs and

associated plots using custom R-scripts (data and R-scripts can be found at https://gitlab.mpcdf.mpg.de/g-adamrunions/growthanalysisscript_zhang_et_al).

For each leaf primordium, segmented leaf surfaces at 2 and 7 DAI were used to quantify blade development based on lineage tracking information. MorphoGraphX was used to calculate clone area at 2 and 7 DAI, as well as growth parameters over the time interval of 2-7 DAI (area extension, proliferation and anisotropy; as described in [31]). To estimate the PD-position of each clone, the distance of the clone from the leaf base was computed at 2DAI (in microns) using Dijkstra's algorithm. The organ aligned directions used for growth analysis (Figures 4N–4P and S4N–S4P) were estimated at 2 DAI, when primordia are relatively radially symmetric. A line was used to approximate the PD-axis of the primordium. For each primordium, this line was placed to pass through the cell at the distal leaf tip as well as the center of the primordium base. For each cell in the abaxial leaf surface, the Medial-Lateral (ML) direction was determined by the vector orthogonal to the PD-axis which was tangent to the surface. For the Proximo-Distal (PD) direction, the vector tangent to the surface and orthogonal to the ML-direction was used. Organ aligned growth rates were determined using the growth tensor [53, 54] calculated for each cell. The growth tensor characterizes a cells 2D expansion over time, and was evaluated in the ML and PD directions to determine organ aligned growth rates. Finally, clones contributing to the leaf blade were marked by tracing the clones of leaf blade at 7DAI back to 2DAI. The list of clones comprising the primordium blade, as well as distances and other values computed in MorphoGraphX were exported as csv files.

Growth alignments for each primordium were created using a custom R-Script. The script loads the csv files exported from MorphoGraphX and eliminates invalid data-values. Normalized PD positions for each clone in a primordium are obtained using percentiles of the distance from leaf base at 2 DAI. Clones are divided into 7-bins based on their normalized PD-position, resulting in approximately the same number of clones in each bin. To obtain growth alignments for average proliferation, area extension, PD/ML growth and anisotropy we use bin-wise averaging (Figures 4J, 4K, 4N–4P, and 4R). By contrast, growth alignments for relative areal and cellular contribution (Figures 4L and 4M) allow the relative contribution of equivalently sized regions along the PD-axis to be evaluated. As in [3], the relative cellular contribution of cells in the i^{th} bin at 2 DAI to the blade at 7 DAI is estimated using the formula:

$$CC = C_{init}/C_{clones}C_{final}$$

where C_{init} is the number of cells in the bin at 2 DAI, C_{final} is the number cells in the bin at 7 DAI and C_{clones} was the total number of clones present at 7 DAI. This estimate corrects for clones present at 2 DAI, which were not captured at all intermediate time-points. To compute relative areal contribution, clones were binned along the PD-axis based on their cumulative area at 2 DAI, binning the primordium into regions accounting for approximately the same total area. Using this binning, relative areal contribution is computed using a similar formula to that of cellular contribution, where C_{final} is replaced by the total area of the cells in a bin at 7 DAI. Both relative cellular and areal contributions are converted to percentages prior to further analysis and plotting.

Growth alignment graphs were plotted in R, using ggplot (n = 3 for each background, 7 PD-percentile positions). To estimate average alignments in each background (Figures 4J–4P and 4R), a cubic orthogonal polynomial was fit to the 21 (PD-percentile, value) pairs for each background. Cubic polynomials were used as a common model for all data, as they capture curvilinear trends in the data without overfitting. PCA analysis was performed in R using prcomp with centering and scaling (stats package) and plotted using ggbiplot (Figures S4J–S4P).

Auxin metabolite quantification

F1or endogenous auxin and its metabolites quantification, approximately 20mg of aerial parts of 2-week-old seedlings were collected for each biological replicate. The plants were frozen immediately in liquid nitrogen after harvest and stored in −80°C upon further experimentation. Extraction was performed according to Dobrev and Kaminek [55]. Briefly, frozen samples with added internal standards (Olchemim, Czech Republic) were extracted and homogenized by bead mill (MixerMill, Retsch GmbH, Haan, Germany) and underwent subsequent solid-phase extraction using MCX cartridges (30mg 1cc, Waters, Milford MA, USA). The obtained eluates were then evaporated to dryness using a SpeedVac and dissolved in 40 μL of 10% methanol. Twenty microliters of each sample were then analyzed by a liquid chromatography–mass spectrometry (LC-MS/MS) system comprising of 1290 Infinity Binary LC System coupled to 6490 Triple Quad LC/MS System with Jet Stream and Dual Ion Funnel technologies, using Mass Hunter software (Agilent Technologies, Santa Clara, CA, USA). The LC-MS/MS system parameters were optimized according to Novák et al. [25] and the concentrations were calculated using a standard isotope dilution method. All solvents used were of analytical or higher grade (SigmaAldrich-Merck GmbH, Steinheim, Germany).

QUANTIFICATION AND STATISTICAL ANALYSIS

Statistical analysis was performed using R and boxplots in Figures 1G, 1H, 2O, 2P, 3R, 3S, S3T, S4F, and S4G were used to visualize data distribution. Error bars in Figure 2C represent standard deviation. All statistical tests and the numbers of how many samples have been analyzed (n) have been indicated in figure legends. The significance threshold used was $p < 0.05$. Leaf contour shape-space plots in Figures 1F, 2N, 3Q, S3S, and S4E were created in LeafI (STAR Methods) based on Principle Component Analysis. PC1 and PC2 values for each contour (colored dots) were respectively plotted along the x- and y axis as multiples of their respective standard deviations (% of explained variance is indicated). Crosses indicate genotype means; Ellipses indicate half the standard deviation.